Sandpile toppling on Penrose tilings: identity and isotropic dynamics

Jérémy Fersula[1], Camille Noûs[2], and Kévin Perrot[1]

[1]Université publique
[2]Cogitamus laboratory

Abstract

We present experiments of sandpiles on grids (square, triangular, hexagonal) and Penrose tilings. The challenging part is to program such simulator; and our javacript code is available online, ready to play! We first present some identity elements of the sandpile group on these aperiodic structures, and then study the stabilization of the maximum stable configuration plus the identity, which lets a surprising circular shape appear. Roundness measurements reveal that the shapes are not approaching perfect circles, though they are close to be. We compare numerically this almost isotropic dynamical phenomenon on various tilings.

Preamble

The experiments presented in this paper were conducted using *JS-Sandpile*, a javascript sandpile simulator we developed. The code is available at

> https://github.com/huacayacauh/JS-Sandpile,

and it is ready for the reader to play at

> https://huacayacauh.github.io/JS-Sandpile/.

The color codes of all our pictures are a gradation, from *almost white* = 0 grain, to *almost black* = $deg(v) - 1$ grains (for any vertex v), *i.e.* the darker it is, the closer to the stability threshold. Stable vertices have greyscale colors, and unstable vertices have flashy colors. Table 1 presents the color codes.

$deg(v)$	0 grain	1 grain	2 grains	3 grains	4 grains	5 grains	6 grains	7 grains
3								
4								
6								

Table 1: Color codes of the pictures in this article, according to the degree of the vertices (all our tilings have the same degree for all its tiles/vertices).

1 Introduction

It all started in 1987 with the work of Bak, Tang and Wiesenfled [2]. Sandpiles have initially been introduced as number conserving cellular automata on the two dimensional square grid, defined by the local toppling of sand grains to neighboring cells, with statistics on chain reactions presenting scale invariance typical of phase transition phenomena in physics, the so called *self-organized criticality* [3, 34]. Soon after, Dhar realized that sandpiles have a beautiful algebraic structure, which generalizes to graphs and digraphs [10]. Since then, sandpiles have raised great interests for their simple local definitions exhibiting complex global behaviors. Following the work of Goles [23], numerous researches have been conducted on one-dimensional models under sequential update mode [24, 25, 32, 50], parallel update mode [13], and some variants such as symmetric [17, 20, 49, 51] or Kadanoff rule [48].

On the two-dimensional side, the identity of the sandpile group on square grids retains its mysteries, though the relaxation of hourglasses (toppling from a single site) begin to reveal its structure through involved partial differential equation developments [35, 36, 37, 44, 45].

The sandpile model on graphs is general enough to embed arbitrary computation, as attested by its Turing-universality [27]. In order to analyse the apparent complexity of the model in a formal framework, particular interest has been raised on the computational complexity of predicting the dynamics of sandpiles. Despite strong efforts started with Moore and Nilsson in [42] and important contributions from Goles, the computational complexity of the problem on two dimensional grids remains open between NC and P. The one-dimensional model is in NC [40, 42], as well as the Kadanoff rule [16, 18] and more general variants [19]. It is P-complete from dimension three [42], and even allows for some undecidable problems [6]. The (im)possibility of building crossing gates in two dimensions is studied in [22, 43], and similar issues on closely related threshold automata such as the majority rule have been fruitful [26, 28, 29, 30, 31, 41]. See [21] for a survey of the results on lattices.

Achieving isotropy in a cellular automaton is not a trivial matter, as cells evolve on intrinsically anisotropic supports (grids). The authors of [9] manage to build parabolas and circles in a two-dimensional cellular automaton with 5^{13} states. Though optimizing the number of state was not an objective of their work, it reflects the difficulty of the task. Approximative (and simpler) approaches to build circles (isotropic diffusion) include: probabilistic methods [39, 54, 55, 58], using a continuous state space [38], or a large neighborhood to alleviate the anisotropy [14, 56, 59].

We give the definition of the sandpile model on general graphs in Section 2, and present its algebraic structure at the heart of the experiments conducted in this article. We also define the tilings considered as supports for the sandpile dynamics: square, triangular and hexagonal grids, Penrose tilings (kite-dart and rhombus) obtained by substitution, and Penrose tilings (rhombus) obtained by the cut and project (multigrid) method. Identity elements of the sandpile group on Penrose tilings are exposed in Section 3. Our main contribution is in Section 4, where we study numerically the isotropy

observed during the stabilization process from the maximum stable configuration plus the identity.

2 Model

Bak, Tang and Wiesenfeld first defined in [2] the sandpile model on two-dimensional grids with von Neumann neighborhood. We present in Subsection 2.1 a general definition on any undirected multi graph, in Subsection 2.2 the algebraic structure first revealed by Dhar in [10], and in Subsection 2.3 we introduce various grids and more generally tilings on which the sandpile model can be studied.

2.1 Sandpiles on graphs

Given a (connected) finite undirected multi graph $G = (V, E)$ with a distinguished *sink* $s \in V$, let $\tilde{V} = V \setminus \{s\}$. A *configuration* $c : \tilde{V} \to \mathbb{N}$ assigns a number of sand grains to each non-sink vertex of G. The basic local evolution rule is the *toppling* at some vertex $v \in \tilde{V}$, which may occur when $c(v) \geq deg(v)$, and consists in vertex v giving as many grains as it has edges to each of its neighbors. When $c(v) \geq deg(v)$ we say that vertex v is *unstable*, and a configuration with no unstable vertex is called *stable*. Formally, let $\Delta = D - A$ be the *graph Laplacian* of G, *i.e.* with D the degree matrix having $deg(v)$ on the diagonal and A the adjacency matrix of G, and let $\tilde{\Delta}$ be the *reduced graph Laplacian* obtained from Δ by deleting the row and column corresponding to the sink s. With $\tilde{\Delta}_v$ the row of $\tilde{\Delta}$ corresponding to vertex $v \in \tilde{V}$, performing a toppling at v corresponds to going from c to $c' = c - \tilde{\Delta}_v$, which we denote $c \xrightarrow{v} c'$, or simply $c \to c'$, and $\to^*$ its reflexive-transitive closure.

As such the system is non-deterministic on configuration space $\mathbb{N}^{\tilde{V}}$, but it is straightforward to notice that any configuration c converges (because of the absorbing sink vertex s) to a unique (because topplings commute) stable configuration, denoted c°. This is the so called *abelian property* of sandpiles, or *fundamental theorem* of sandpiles. The vector x such that $c - \tilde{\Delta} \cdot x = c^\circ$ is called the *shot vector* or *odometer function* of configuration c, it records how many times each vertex has toppled during the *stabilization* of c. The fundamental theorem of sandpiles furthermore states that the odometer function of any configuration is unique.

For the purpose of simulations that take some importance in the present work, we define the deterministic *synchronous* dynamics as the evolution toppling synchronously all unstable vertices, at each step. Formally, we define $c \Rightarrow c'$ with

$$c' = c - \sum_{\substack{v \in \tilde{V} \\ c(v) \geq deg(v)}} \tilde{\Delta}_v.$$

An example is given on Figure 1. For the sake of simplicity, in the following *graph* will stand for *finite undirected multi graph*.
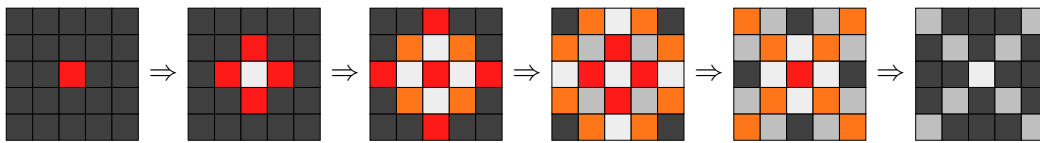
Figure 1: Five steps of the sandpile model on a square grid of size 5×5, corresponding to the graph with one vertex per square and north-east-south-west adjacencies (all vertices have degree 4). The sink s is not pictured, squares/vertices on the border have one edge connected to s, and squares/vertices on the corners have two edges connected to s.

2.2 Abelian group structure

Given a graph $G = (V, E)$ with sink s, let $\mathcal{C} = \mathbb{N}^{\tilde{V}}$ denote its set of configurations. The set of *stable configurations* $\mathcal{C}_{\texttt{stab}}$ is naturally equipped with the *operation* $\oplus$ defined as

$$c \oplus c' = (c + c')^{\circ}$$

where $c + c'$ is the componentwise addition of two configurations, *i.e.* $(c + c')(v) = c(v) + c'(v)$ for all $v \in \tilde{V}$. It is straightforward to notice that $(\mathcal{C}_{\texttt{stab}}, \oplus)$ is a *commutative monoid* (closure, associativity, identity, commutativity), the identity being the configuration z such that $z(v) = 0$ for all $v \in \tilde{V}$.

Here comes the magics of sandpiles. The set of *recurrent configurations*

$$\begin{aligned}
\mathcal{C}_{\texttt{rec}} &= \{c \in \mathcal{C}_{\texttt{stab}} \mid \forall c' \in \mathcal{C} : \exists c'' \in \mathcal{C} : c' \oplus c'' = c\} \\
&= \{c \in \mathcal{C}_{\texttt{stab}} \mid \forall c' \in \mathcal{C}_{\texttt{stab}} : \exists c'' \in \mathcal{C}_{\texttt{stab}} : c' \oplus c'' = c\}
\end{aligned}$$

corresponds to the intersection of ideals of $\mathcal{C}_{\texttt{stab}}$, *i.e.*

$$\mathcal{C}_{\texttt{rec}} = \bigcap_{\substack{I \subseteq \mathcal{C}_{\texttt{stab}} \\ I \text{ ideal of } \mathcal{C}_{\texttt{stab}}}} I$$

with I (right) *ideal* of $\mathcal{C}_{\texttt{stab}}$ if and only if $I \oplus \mathcal{C}_{\texttt{stab}} \subseteq \mathcal{C}_{\texttt{stab}}$ where $I \oplus \mathcal{C}_{\texttt{stab}} = \{i \oplus c \mid i \in I \text{ and } c \in \mathcal{C}_{\texttt{stab}}\}$. Moreover, it is a classical result of algebra that the intersection of all ideals of a *commutative semigroup* (closure, associativity, commutativity) gives an *abelian group* (closure, associativity, identity, inverse, commutativity). So $(\mathcal{C}_{\texttt{rec}}, \oplus)$ is an abelian group, called the *sandpile group* on graph G with sink s. Now remark that the configuration z containing no grain is (except on very restricted cases) not an element of $\mathcal{C}_{\texttt{rec}}$, hence the[1] identity element $e \in \mathcal{C}_{\texttt{rec}}$ of the sandpile group is *a priori* not obvious to construct, and it turns out that few is know about its structure on numerous interesting cases, as presented on Figure 2. It can be proven that

$$e = (2m - (2m)^{\circ})^{\circ} \tag{1}$$

with m the *maximum stable* configuration defined as $m(v) = deg(v) - 1$ for all $v \in \tilde{V}$, and $(2m)(v) = 2\,c(v)$ for all $v \in \tilde{V}$. Indeed, $2m - (2m)^{\circ}$ contains at least $deg(v) - 1$ grains at

---

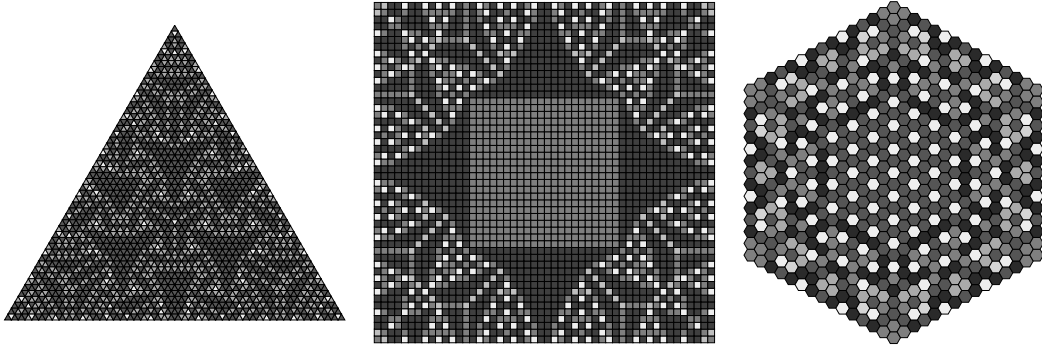[1] The identity element of the sandpile group is unique.

4

Figure 2: Identity elements of the sandpile group on graphs corresponding to the triangular grid of side length 50 (left, $deg(v) = 3$ for any vertex v), the square grid of side length 50 (center, $deg(v) = 4$ for any vertex v), the hexagonal grid of side length 14 (right, $deg(v) = 6$ for any vertex v). All at the same scale.

each vertex $v \in \tilde{V}$ hence its stabilization is recurrent, and furthermore it corresponds to subtracting two configurations from the same equivalence class according to relation $\leftrightarrow^*$ (the symmetric closure of $\rightarrow^*$), therefore to a configuration in the class of the identity (see [11] for details). The equality follows since the identity element of $(\mathcal{C}_{\texttt{rec}}, \oplus)$ is unique.

2.3 Tilings

We will concentrate on finite tilings, but still introduce general definitions. An *infinite tiling* $\mathcal{T}$ by τ is a covering of $\mathbb{R}^2$ by finitely many polygonal *tiles* and their images by isometry (translation, rotation, flip), *i.e.* copies of the tiles from τ cover the plane without gaps nor overlaps. Let τ be a finite set of polygonal tiles called a *tile set*, then $\mathcal{T}$ is a partition of $\mathbb{R}^2$ into countably many isometries of the elements from τ.

An infinite tiling $\mathcal{T}$ is *periodic* when it has a non-null periodicity vector $\vec{p} \in \mathbb{R}^2$, such that $\mathcal{T} + \vec{p} = \mathcal{T}$. A tile set τ is *aperiodic* when it admits at least one infinite tiling (we say that τ *tiles the plane*), and none are periodic. Aperiodicity is fundamentally related to the uncomputability of the *domino problem*: given a (finite) tile set, does it tile the plane? Let us quickly mention the seminal contributions of Wang [57], Berger [5] and Robinson [52], along with the book *Tilings and Patterns* by Grünbaum and Shephard [33].

In order to consider sandpiles on tilings, we explain now how to construct finite undirected multi graphs with a distinguished sink. A *finite tiling* is simply a subset of some infinite tiling $\mathcal{T}$. Remark that this requires a finite tiling to be *extensible* into an infinite tiling, which will be the case for all our finite tilings. Indeed, given some tile set τ we will generate arbitrarily large finite tilings, which implies the existence of an infinite tiling by compactness of the set of infinite tilings by τ. Two tiles are *adjacent* in $\mathcal{T}$ when they share an edge. All the tilings we consider will see their adjacent tiles share full sides, *i.e.* no tile will share a partial side or more than one side with another

tile. These are called *edge-to-edge* tilings. Given a finite tiling, each tile corresponds to a vertex, plus an additional sink vertex corresponding to the *outside face*. The tile to tile adjacencies are given by the edge-to-edge connections, and the number of edges connecting a tile to the sink is equal to its number of sides connected to the outside face, so that the degree of every tile is equal to its number of sides. Tiles connected to the sink are said to be on the *border* of the Tiling. Note that the sandpile dynamics is given by this underlying graph, but tiles furthermore have coordinates in $\mathbb{R}^2$.

We now present the finite tilings considered in this article. The size of tiles and the position of coordinate $(0, 0)$ will be important for the observations presented in Section 4. Grids are illustrated on Figure 2.

Square grids. They correspond to the original two-dimensional sandpile model by Bak, Tang and Wiesenfled [2]. Given size n, it basically consists in a $n \times n$ square grid with adjacencies given by von Neumann neighborhood (north, east, south, west). Tiles on the borders have one edge connected to the sink, and tiles on the corners have two edges connected to the sink. Each tile is a square of side length 1, and the finite tiling is centered with coordinate $(0, 0)$ in the middle of the grid: if n is even then coordinate $(0, 0)$ corresponds to four tiles corners; otherwise coordinate $(0, 0)$ corresponds to the center of a tile.

Triangular grids. Given size n, it is made of equilateral triangles of side length 1, arranged up and down to form an equilateral triangle of side length n, where the three outer sides of the tiling are made of n triangular tiles. Tiles on the border have one edge connected to the sink, and tiles on the corners have two edges connected to the sink. The finite tiling is centered with coordinate $(0, 0)$ at the barycenter of its three corners.

Hexagonal grids. Given size n, it is made of regular hexagons of side length 1, arranged to form an hexagonal grid (orientation is *flat*) with six sides each made of n tiles. Tiles on the border have two edges connected to the sink, and tiles on corners have three edges connected to the sink. The finite tiling is centered with coordinate $(0, 0)$ at the center of the central hexagon.

Penrose tilings. Penrose developed in [46, 47] a series of elegant aperiodic tile sets. We consider *P2* (*kite-dart*), and *P3* (*rhombus*) (tilings by P2 and P3 are *mutually locally derivable*, see [1]). Penrose tilings may be obtained by *substitution*[2] as described on Figure 3 for P2, and Figure 4 for P3. After substituting, we rescale all tiles up by the substitution factor $\phi = \frac{1+\sqrt{5}}{2}$, so that the tiles of the final tiling have the exact same size as the base tiles (kite, dart, fat, thin). Figure 5 presents three iterations of the substitution from a *P2 Sun*, Figure 6 presents three iterations of the substitution from a *P2 Star*, and Figure 7 presents three iterations of the substitution from a *P3*

---

[2]Note that in order to enforce aperiodicity in P2 and P3, matching constraints should be added on tile edges, for example via notches, but the finite tiling generation methods we employ do not require such considerations.
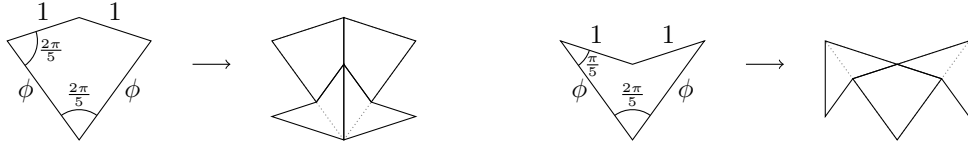
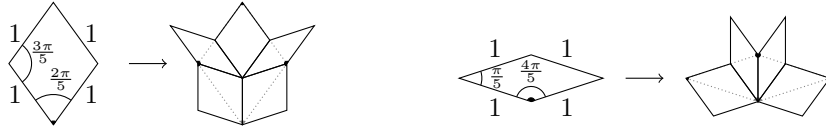Figure 3: Substitutions of P2 kite (left) and dart (right) tiles.

Figure 4: Substitutions of P3 fat (left) and thin (right) rhombi tiles. Due to the symmetry of P3 tiles, we highlight the origin point of each tile.

Sun. Coordinate $(0,0)$ is at the center of the initial Suns and Stars, and remains at the symmetry center of tilings obtained by subsequent substitutions.

Penrose P3 tilings may alternatively be generated by *cut and project* method: consider the 5-dimensional plane E spaned by vectors $(\cos \frac{2k\pi}{5})_{0 \le k < 5}$ and $(\sin \frac{2k\pi}{5})_{0 \le k < 5}$, passing through the point $(\frac{1}{5}, \frac{1}{5}, \frac{1}{5}, \frac{1}{5}, \frac{1}{5})$. The orthogonal projection of the 5-dimensional grid lines (1-simplices) contained in $E + [0,1]^5$ onto E gives a tiling by P3 tiles. We implement it via the dual *multigrid* method of de Bruijn [8], where one considers a 2-dimensional space and five line families (our *pentagrid*) given by the intersections of E with the five 5-dimensional hyperplanes $G_i = \{x \in \mathbb{R}^5 \mid x \cdot e_k \in \mathbb{Z}\}$ for $0 \le k < 5$, where e_k is the k-th unit vector of $\mathbb{R}^5$. Pentagrid lines of a family are *indexed* by the value of $x \cdot e_k$, and we denote ℓ_i^k the line from family $0 \le k < 5$ of index $i \in \mathbb{Z}$. Note that with this setting, no more than two pentagrid lines intersect at a given position. The 2-dimensional space is divided into polygonal *cells* delimited by pentagrid lines. Each cell p is labeled by a 5-tuple of integers $(p_k)_{0 \le k < 5}$ such that cell p lies in between lines $\ell_{p_k}^k$ and $\ell_{p_k+1}^k$. To each cell p corresponds a point (a tile's bound coordinate) in the 2-dimensional space, at $\sum_{0 \le k < 5} p_k (\cos \frac{2k\pi}{5}, \sin \frac{2k\pi}{5})$. It follows that to each intersecting pair of pentagrid lines corresponds a tile, whose two edge orientations are given by the two line families. Details can be found in [15]. We bound this process to a finite *P3 cut and project tiling of size n* by considering only tiles corresponding to points of intersection lying in between ℓ_{-n}^i and ℓ_n^i for all families $0 \le i < 5$. The coordinate $(0,0)$ of this tiling is given by the cell labeled $(0,0,0,0,0)$, and is therefore a tile bound (shared by multiple tiles). Rhombus tiles have side length 1 as on Figure 4. Figure 8 presents some P3 cut and project tilings.
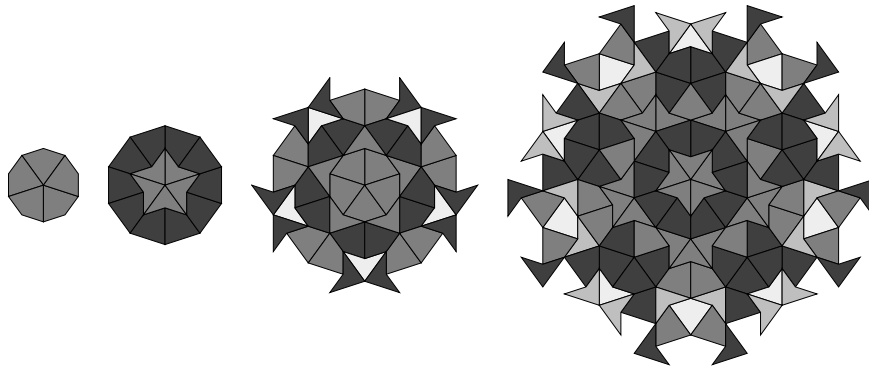
Figure 5: Three iterations of the susbtitution from a *P2 Sun*, with identity elements of the sandpile group pictured.
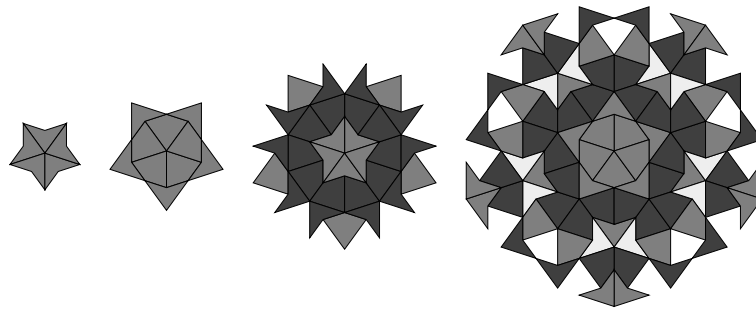

Figure 6: Three iterations of the susbtitution from a *P2 Star*, with identity elements of the sandpile group pictured.
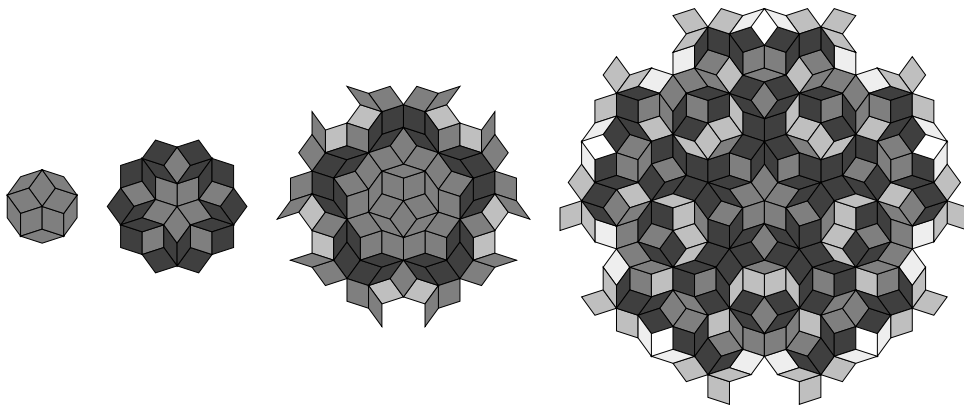

Figure 7: Three iterations of the susbtitution from a *P3 Sun*, with identity elements of the sandpile group pictured.
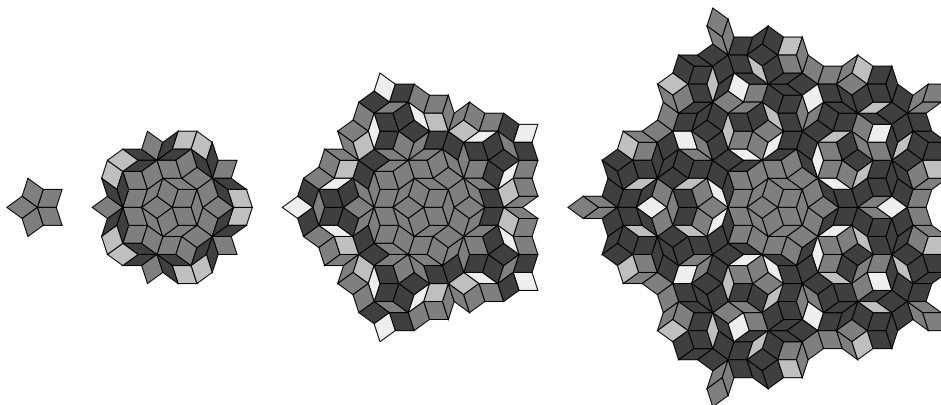
Figure 8: P3 cut and project tilings of sizes 1, 2, 3 and 4, with identity elements of the sandpile group pictured.

3 Sandpile identity on Penrose tilings

We were curious to see what the identity element of the sandpile group would look like on (finite) Penrose tilings, and it seems that no particular structure appears[3]. Examples are presented on Figures 9, 10 and 11, *JS-Sandpile* computes them from Formula 1.

We nevertheless discovered an interesting phenomenon on P3 cut and project tilings, where the identity elements seem to display some stability. Indeed, identity elements on successive sizes have a somewhat large central part of the configuration in common. This obeservation is presented on Figure 12. We may therefore conjecture a convergence of the sandpile identity on P3 cut and project tilings: as the size n increases, a larger part of the identity is fixed (remains the same for all sizes $n' \geq n$). Let us remark that this phenomenon does not seem to take place on P2 nor P3 tilings obtained by subsitution.

4 Isotropic dynamics

On square, triangular, hexagonal grids and Penrose tilings, a very interesting phenomenon appears[4] during the stabilization process

$$(m + e)^\circ = m$$

where m is the maximum stable configuration ($m(v) = deg(v) - 1$ for all tile v) and e is the identity element of the sandpile group. Indeed, during the last phase of the stabilization process leading back to m (which is a uniform configuration in these cases since the number of neighbors is identical for all tiles), one can see the configuration m reappear from the outside (near the border) towards the center, outside a shrinking circular shape, in a process step by step covering the whole configuration with tiles

---

[3]Well, this is a bit disappointing, but we think that it is worth showing that it does not appear to be a fruitful research direction, or maybe a more insightful reader would encounter something out there...

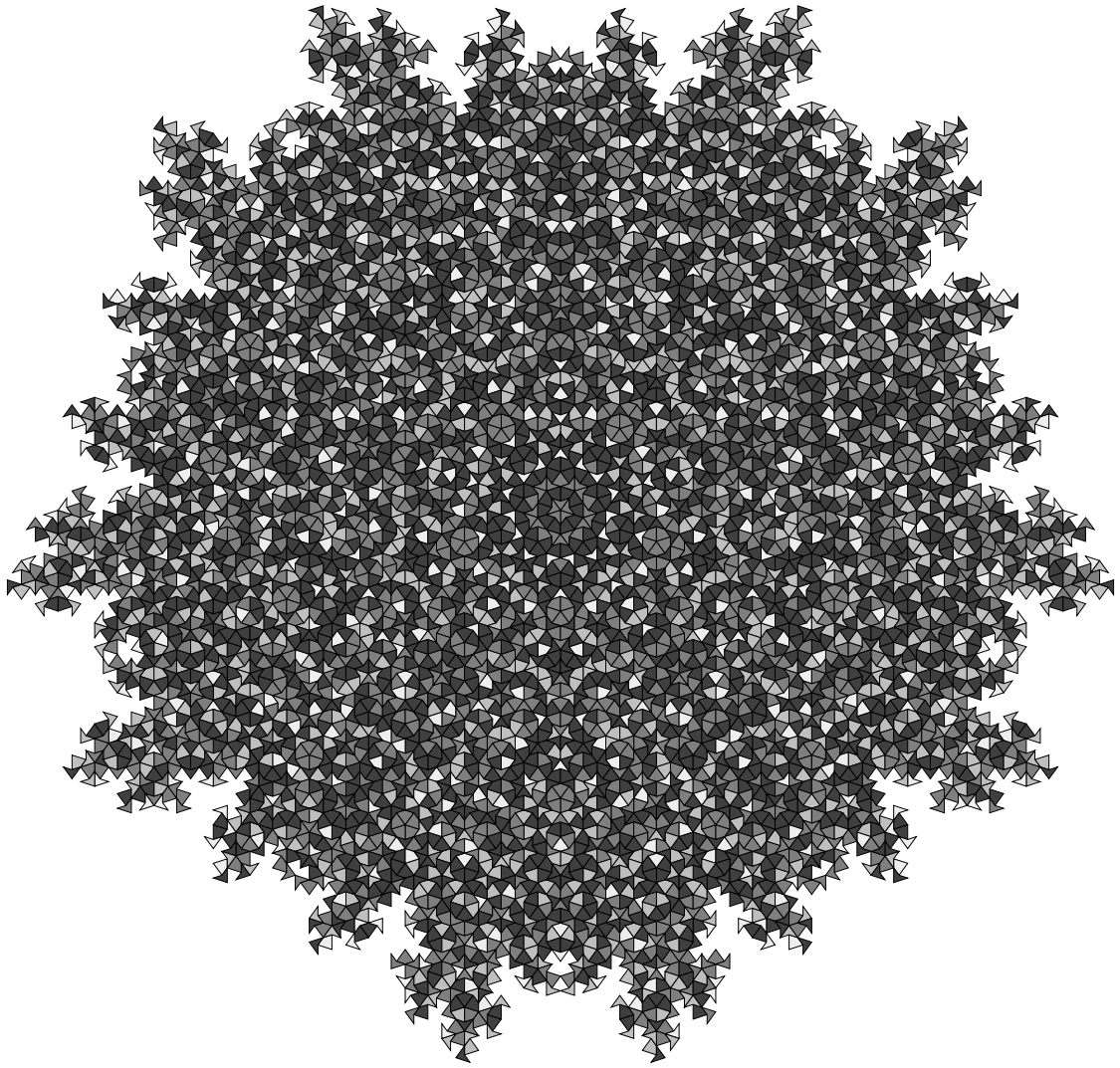[4]This also takes place on other tilings, outside the scope of the present work.

Figure 9: Identity element of the sandpile group on the tiling obtained after 7 iterations of the substitution from a P2 Sun (6710 tiles).
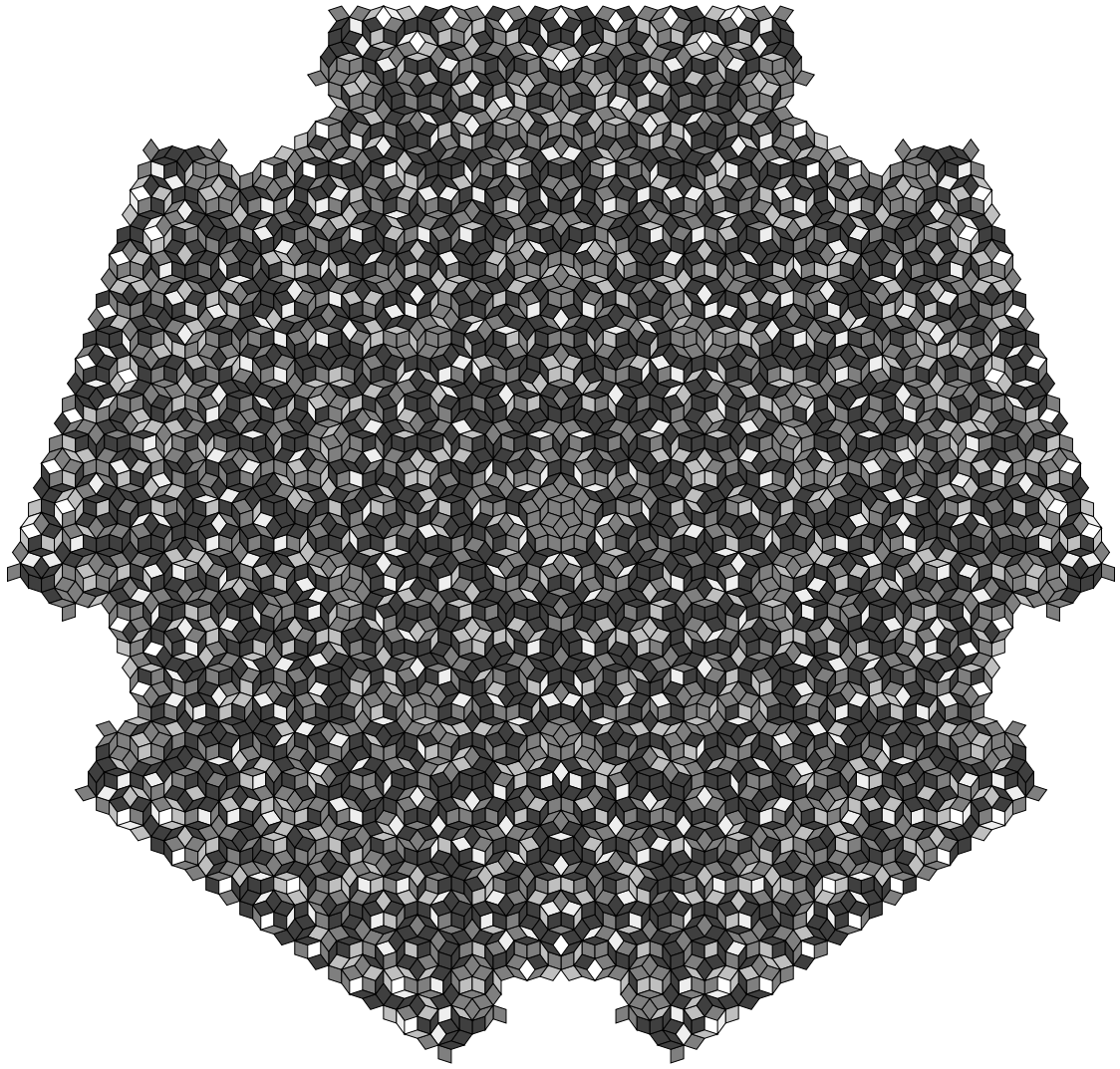
Figure 10: Identity element of the sandpile group on the tiling obtained after 6 iterations of the substitution from a P3 Sun (5415 tiles).
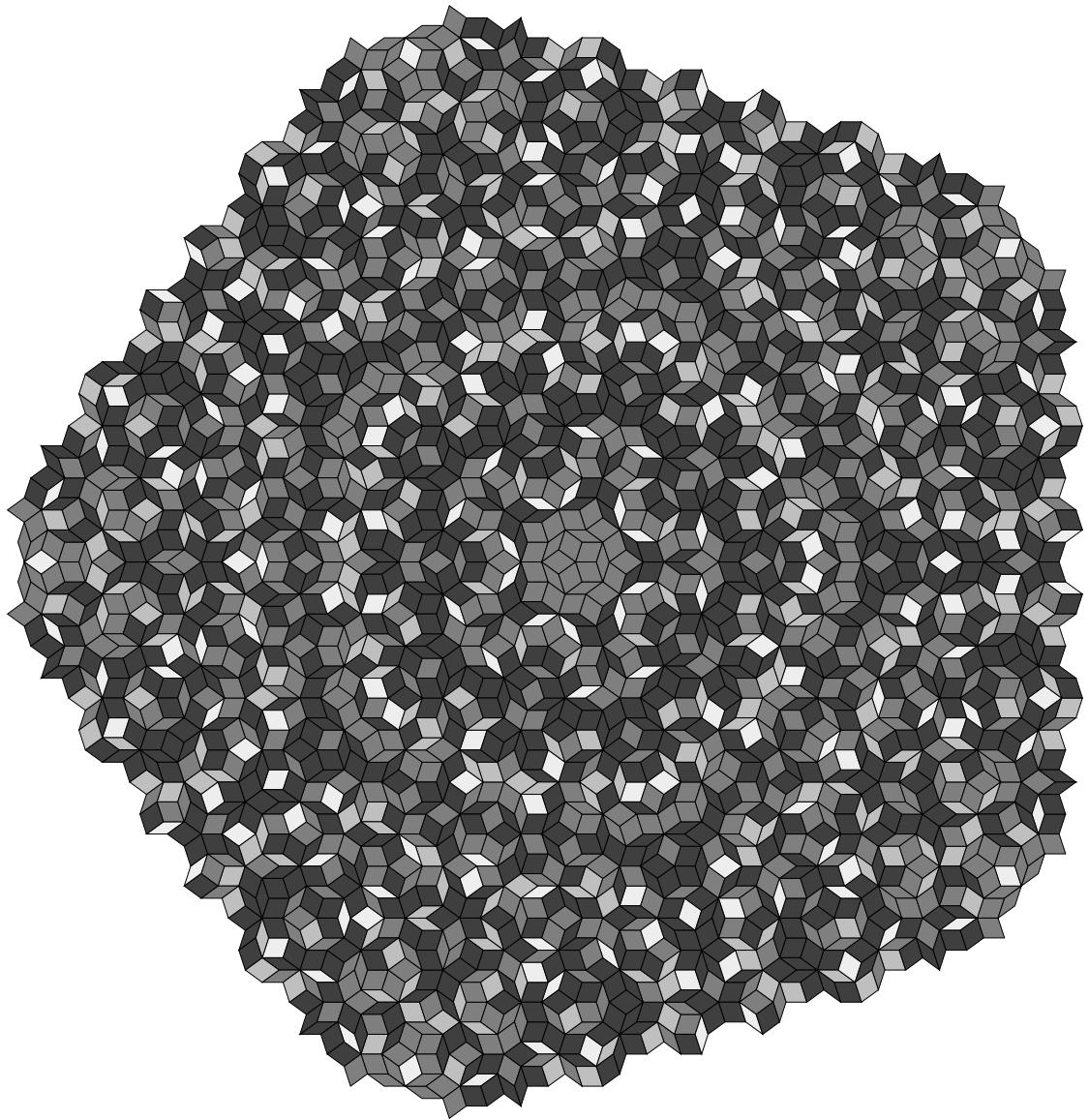
Figure 11: Identity element of the sandpile group on a P3 cut and project tiling of size 10 (2440 tiles).
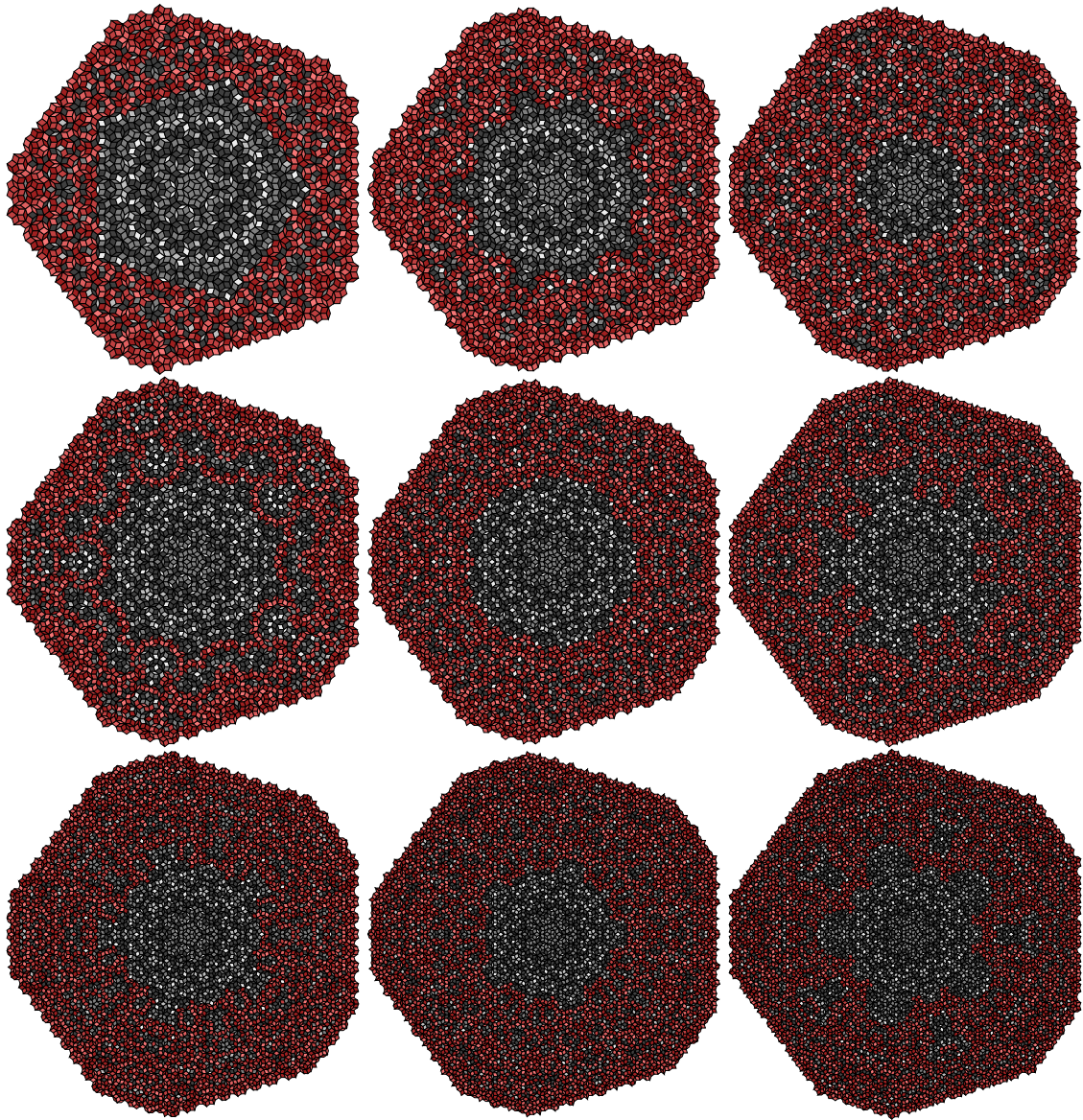
Figure 12: Differences between successive identity elements of the sandpile group on P3 cut and project tilings. From left to right, top to bottom, are displayed the identity elements on P3 cut and project tilings of sizes 11 (2900 tiles), 12 (3520 tiles), 13 (4155 tiles), 14 (4790 tiles), 15 (5570 tiles), 16 (6250 tiles), 17 (7140 tiles), 18 (8080 tiles), 19 (8890 tiles) and 20 (9940 tiles), where the part of the configuration which differs from the previous size (sizes n is compared to size $n-1$) are highlighted with redshifted colors.
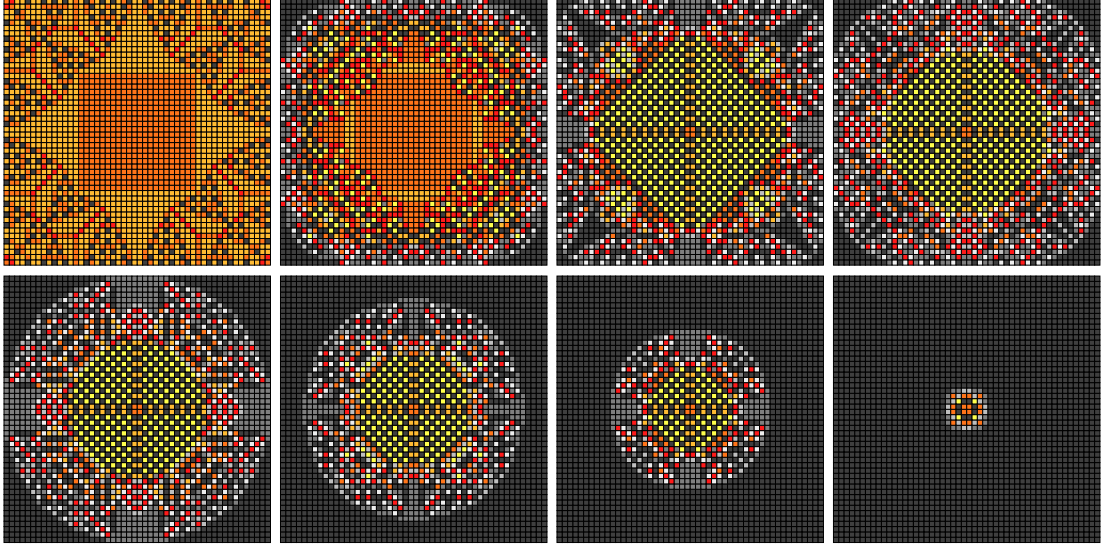
Figure 13: Stabilization of $(m + e)^\circ = m$ on a square grid of side length 50. From left to right, top to bottom, are displayed the configurations every 100 time steps (starting with $m + e$ at step 0, ending with time step 700). The process converges to m at step 707.

containing $deg(v) - 1$ grains. The first part of the stabilization process is quite involved. Two illustrations are given on Figures 13 and 14.

4.1 Roundness

In order to measure this phenomenon, we introduce the *roundness* as follows. First, we partition a configuration into two parts: the outside part with all tiles having $deg(v) - 1$ grains connected to the border, and the inner part. Given a tiling $G = (V, E)$ with sink s and a configuration $c : \tilde{V} \to \mathbb{N}$, let the *maximum stable components*, $\texttt{MSC}(c) = \{V_1, V_2, \ldots, V_k\}$, be the connected components of tiles (from $\tilde{V}$) having $deg(v) - 1$ grains. Then the *outer tiles* is the set

$$\texttt{outer}(c) = \bigcup_{\substack{V_i \in \texttt{MSC}(c) \\ \exists v \in V_i : \{v, s\} \in E}} V_i$$

and the *inner tiles* is the set $\texttt{inner}(c) = \tilde{V} \setminus \texttt{outer}(c)$. From this partition of the set of tiles, we are interested in the frontier between the outer and inner tiles, and how close it is from a perfect circle. This has to do with the coordinates of tiles in the Euclidean space $\mathbb{R}^2$, so let us denote $\texttt{coord}(v)$ the set of coordinates of the bounds of some tile $v \in \tilde{V}$, and $\texttt{body}(v)$ the subset of $\mathbb{R}^2$ covered by the tile. Our convention regarding the sink s is discussed below. Regarding the circle, let us denote $\texttt{B}(r)$ the inside of the circle
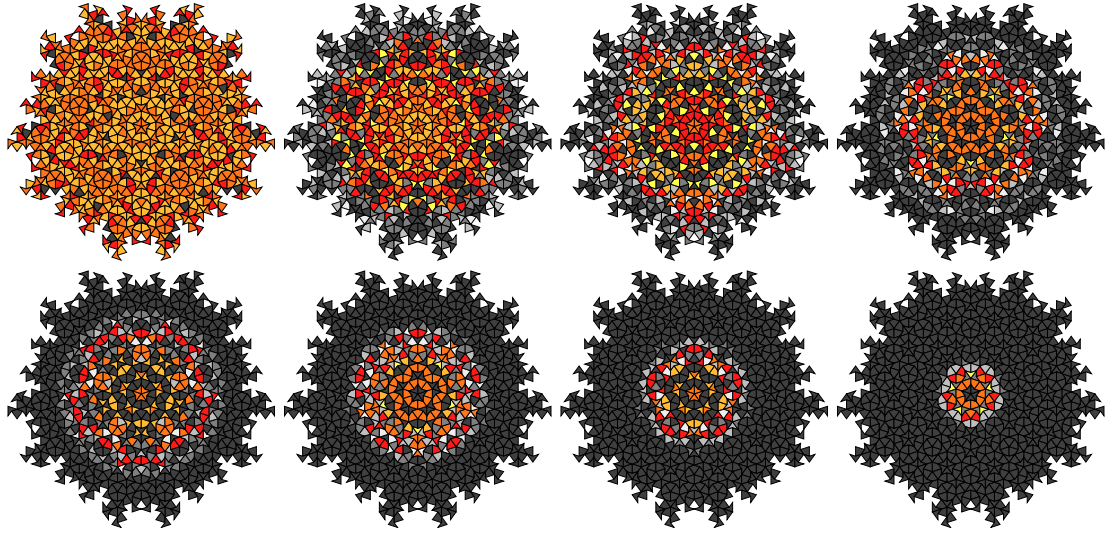
14

Figure 14: Stabilization of $(m + e)^\circ = m$ on 5 iterations of the substitution from a P2 Sun. From left to right, on top are displayed time steps $0, 50, 100, 150$ and at the bottom time steps $165, 180, 195, 210$. The process converges to m at step 220.

of radius $r \in \mathbb{R}$ centered at coordinate $(0,0)$, *i.e.*

$$\mathtt{B}(r) = \{(x, y) \in \mathbb{R}^2 \mid \sqrt{x^2 + y^2} \le r\}.$$

We may therefore denote $\mathtt{body}(v) \cap \mathtt{B}(r) = \emptyset$ to state that tile v is entirely outside the circle of radius r centered at $(0,0)$, and $\mathtt{body}(v) \subseteq \mathtt{B}(r)$ (or equivalently $\mathtt{coord}(v) \subseteq \mathtt{B}(r)$ since we deal with polygons and the circle is convex) to state that tile v is entirely inside the same circle. We define the *outer radius* as the maximum scalar r such that all outer tiles are outside the circle of radius r around the origin $(0,0)$ of the tiling,

$$\underline{\mathtt{r}}(c) = \max\{r \in \mathbb{R}_+ \mid \forall v \in \mathtt{outer}(c) : \mathtt{body}(v) \cap \mathtt{B}(r) = \emptyset\}$$

and the *inner radius* as the minimum scalar r such that all inner tiles are inside the circle of radius r around the origin $(0,0)$ of the tiling,

$$\overline{\mathtt{r}}(c) = \min\{r \in \mathbb{R}_+ \mid \forall v \in \mathtt{inner}(c) : \mathtt{body}(v) \subseteq \mathtt{B}(r)\}.$$

In order to deal with the case $\mathtt{outer}(c) = \emptyset$, which may for example be the case on some configurations $(m + e)$, we add the convention that the sink s is an infinite tile covering all the space outside the tiling, whose coordinates are the union of all bounds from tile edges adjacent to the sink, and that it always belongs to $\mathtt{outer}(c)$. As a consequence the outer radius is upper bounded by the radius of the inscribed circle (inside the finite tiling) with center at $(0,0)$. The case $\mathtt{inner}(c) = \emptyset$ is not problematic since the minimum defining $\overline{\mathtt{r}}(c)$ is taken on $\mathbb{R}_+$, and would therefore equal 0 as expected. The inner radius is upper bounded by the radius of the circumscribed circle (outside the finite tiling) with
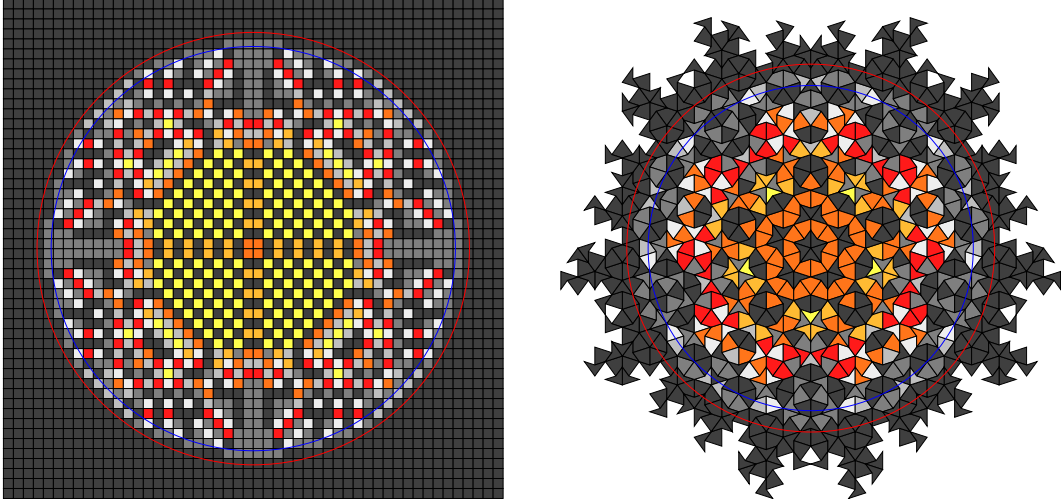
Figure 15: Examples of roundness measures, circles of outer radius $\underline{r}(c)$ in blue, inner radius $\overline{r}(c)$ in red. Left: square grid of side length 50, after 500 steps from $(m + e)$ (converges to m in 707 steps), $r(c) \approx 21.633 - 20.224 = 1.409$. Right: 5 iterations of the substition from a P2 Sun, after 150 steps from $(m + e)$ (converges to m in 220 steps), $r(c) \approx 16.662 - 14.729 = 1.933$.

center at $(0, 0)$. The *roundness of a configuration* c is then measured as the difference between the inner and outer radii,

$$r(c) = \overline{r}(c) - \underline{r}(c).$$

Note that $0 \leq r(c)$, and we have $r(c) = 0$ when the frontier between inner and outer tiles is a perfect circle. Two examples of roundness are given on Figure 15.

4.2 Base roundnesses

Remark that since all our tiles are polygonal (with three to six sides), we cannot expect to reach roundness 0 (except when the stabilization process has converged to m). To get some easy to interpret base values, we consider the diameter of each tile, as the diameter of the circumscribed circle around the tile (smallest radius of a circle having the tile entirely is its interior). See Figure 16. The greatest diameter of some tiling's tiles can be interpreted as an upper bound on the best achievable roundness, for any radius. Indeed, consider some tiling and a circle C (of radius at most equal to the inscribed radius), then all tiles having the center of their circumscribed circle on or outside the circle C can be set as outer tiles, and all tiles having the center of their circumscribed circle inside the circle C can be set as inner tiles, which results in a roundness smaller than twice the radius of the greatest tile's radius, *i.e.* smaller than the greatest tile's diameter. We obtain the *base roundnesses* presented on Table 2.
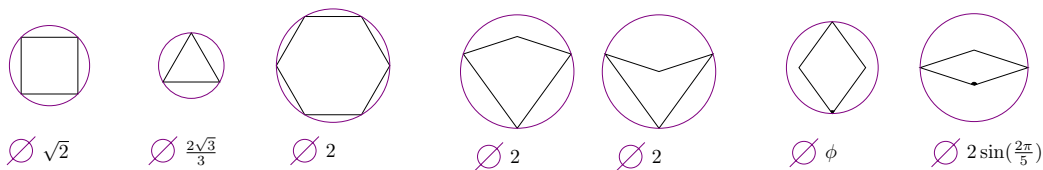
16

Figure 16: Diameters of all tiles, as the diameter of a circumscribed circle (in purple). All tiles at the same scale.

Tiling	Square grids	Triangular grids	Hexagonal grids	P2 tilings	P3 tilings
Base roundness	$\sqrt{2}$ ≈ 1.414	$\frac{2\sqrt{3}}{3}$ ≈ 1.155	2	2	$2\sin(\frac{2\pi}{5})$ ≈ 1.902

Table 2: Base roundnesses as the greatest diameter of some tiling's tiles.

4.3 Plots

We now present plots of roundness measured during the stabilization process $(m + e)^\circ = m$ on the different tilings considered in this article. We decompose the stabilization process from $m + e$ to m into two phases:

○ **phase 1:** the dynamics is erratic,
○ **phase 2:** the set of inner tiles slowly shrinks, until reaching $\texttt{inner}(m) = \emptyset$.

The *beginning of phase 2* is defined as the first step such that the inner radius is smaller or equal to the inscribed radius of the tiling (maximum radius of a circle entirely inside the finite tiling, and centered at the origin). Remark that at the beginning of phase 2, all tiles on the border of the tiling are outer tiles, because the polygonal shape of any inner tile on the border would otherwise lead to the inner radius being greater than the inscribed radius of the tiling. An important observation is that, in all the experiments presented in this article and performed during its preparation, once in phase 2 with all border tiles as outer tiles, then all border tiles *remain* outer tiles[5], and that the inner radius *remains* smaller or equal to the inscribed radius. Two full examples of roundness plots are given on Figures 17, 19, and their companion Figures 18, 20.

Experimental results, picturing only phase 2 of the stabilization process from $m + e$ to m, are presented on Figure 21 and 22. Note that during all the experiments we have performed in preparing this article, we have observed similar behaviors for all other sizes.

---

[5]They all remain stable with $deg(v) - 1$ grains until reaching m. Observe that any outer tile receiving some grain would topple, and that toppling any outer tile would result in toppling the whole maximum stable component it belongs to.
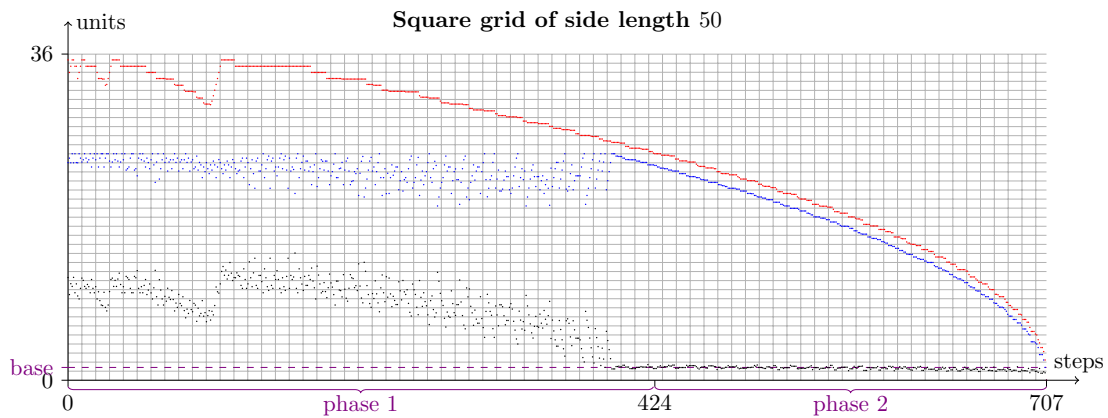
Figure 17: Plot of the roundness during the stabilization process $(m + e)^\circ = m$, on the square grid of side length 50. At each step we plot the inner radius $\bar{\mathbf{r}}(c)$ in red, outer radius $\underline{\mathbf{r}}(c)$ in blue, and roundness $\mathbf{r}(c)$ in black. Grid has one row per unit and one column per 10 time steps. For example, at step 3, with $m + e \Rightarrow c^1 \Rightarrow c^2 \Rightarrow c^3$, we observe that $\bar{\mathbf{r}}(c^3) = 25\sqrt{2} \approx 35.355$ (the radius of the circumscribed circle around the whole tiling) and that $\underline{\mathbf{r}}(c^3) = 25$ (the radius of the inscribed circle inside the whole tiling), so that $\mathbf{r}(c^3) = 25(\sqrt{2} - 1) \approx 10.355$ (at step 0 some outer tiles near the $x = 0$ and $y = 0$ axis give different radii). Phase 2 begins at step 424, and configuration m is reached at step 707. The base roundness of this tiling (dashed) is $\sqrt{2}$. See also the companion Figure 18.
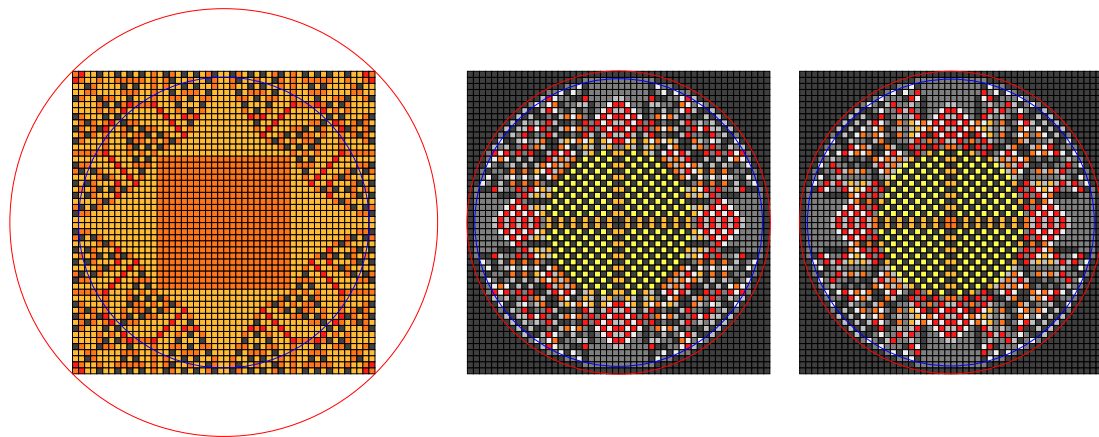

Figure 18: Configurations at steps 0 (this is $m + e$), 423 and 424 during the stabilization process $(m + e)^\circ = m$, on the square grid of side length 50. Inner radii in red, outer radii in blue. One can observe the phase transition occurring at step 424: the inner radius becomes smaller or equal to the inscribed radius of the tiling.
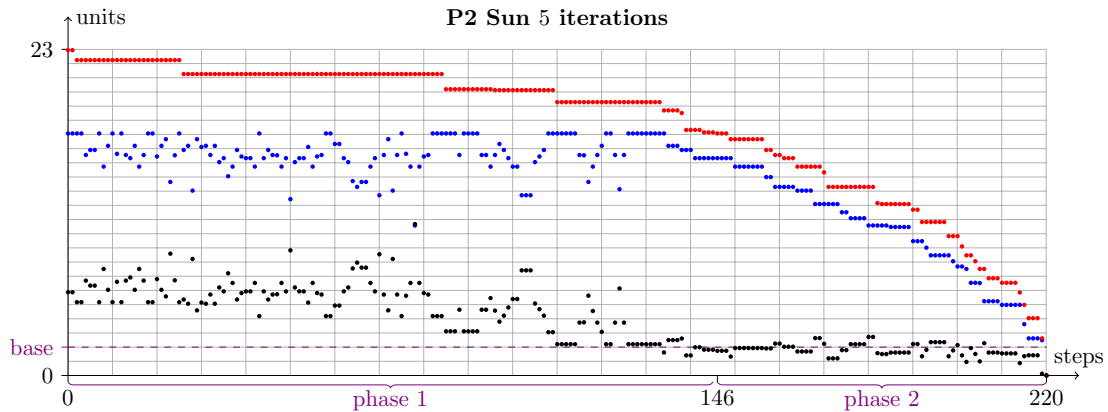
18

Figure 19: Plot of the roundness during the stabilization process $(m + e)^\circ = m$, on the tiling obtained after 5 iterations of the substitution from a P2 Sun. At each step we plot the inner radius $\bar{\mathtt{r}}(c)$ in red, outer radius $\underline{\mathtt{r}}(c)$ in blue, and roundness $\mathtt{r}(c)$ in black. Grid has one row per unit and one column per 10 time steps. For example, at step 0 we observe that $\bar{\mathtt{r}}(m + e) \approx 22.940$ (the radius of the circumscribed circle around the whole tiling) and that $\underline{\mathtt{r}}(m + e) \approx 17.069$ (the radius of the inscribed circle inside the whole tiling), so that $\mathtt{r}(m + e) \approx 5.871$. Phase 2 begins at step 146, and configuration m is reached at step 220. The base roundness of this tiling (dashed) is 2. See also the companion Figure 20.
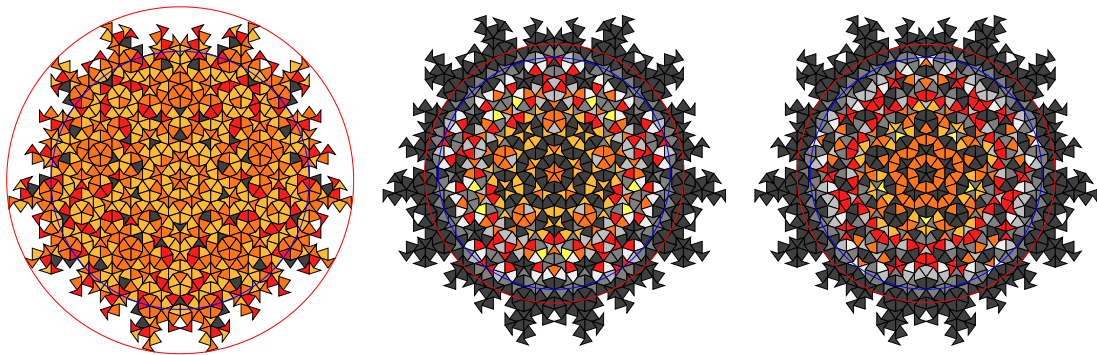

Figure 20: Configurations at steps 0 (this is $m+e$), 145 and 146 during the stabilization process $(m + e)^\circ = m$, on the tiling obtained after 5 iterations of the substitution from a P2 Sun. Inner radii in red, outer radii in blue. One can observe the phase transition occurring at step 146: the inner radius becomes smaller or equal to the inscribed radius of the tiling.
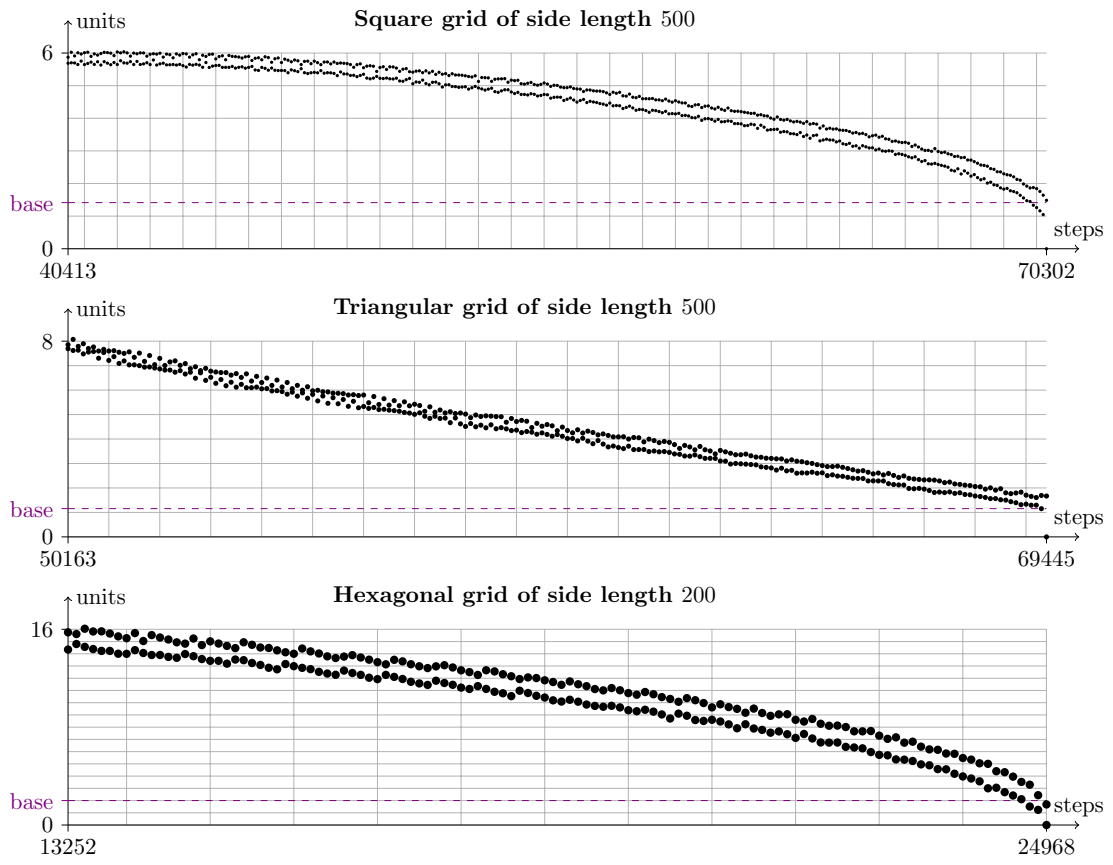
19

Figure 21: Plots of the roundness during phase 2 of the stabilization process $(m + e)^\circ = m$, on the square grid of side length 500, triangular grid of side length 500, and hexagonal grid of side length 200. Grids have one row per unit and one column per 1000 time steps. Two points are drawn every 100 time steps: the maximum and minimum roundness values $\mathbf{r}(c)$ observed among these 100 steps.
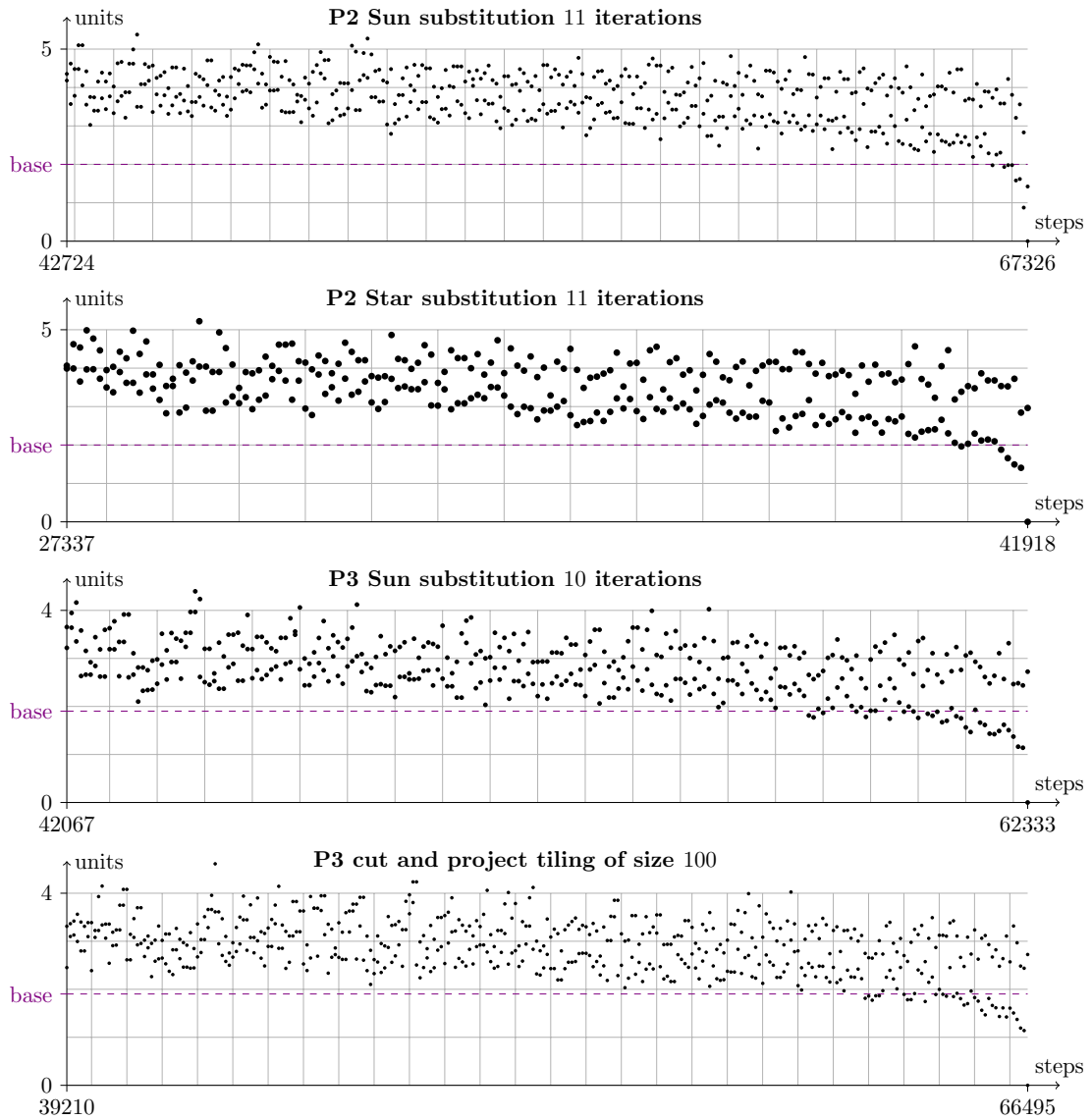
20

Figure 22: Plots of the roundness during phase 2 of the stabilization process $(m + e)^\circ = m$, on the P2 Sun after 11 iterations of the substitution, P2 Star after 11 iterations of the substitution, P3 Sun after 10 iterations of the substitution, P3 cut and project tiling of size 100. Grids have one row per unit and one column per 1000 time steps. Two points are drawn every 100 time steps: the maximum and minimum roundness values $\mathtt{r}(c)$ observed among these 100 steps.

Tiling	Size/ iter.	Tiles	Identity (seconds)	Roundness (seconds)	Phase 2 begin step	Stabilization step
Square grid	500	250000	825	1294	40413	70302
Triangular grid	500	250000	1143	689	50163	69445
Hexagonal grid	200	120601	271	405	13252	24968
P2 Sun subst.	11	327750	2931	1850	42724	67326
P2 Star subst.	11	234410	944	640	27337	41918
P3 Sun subst.	10	266860	2227	1570	42067	62333
P3 cut & project	100	249610	3145	2386	39210	66495

Table 3: Data regarding the computations generating the graphics presented on Figures 21 and 22. Running times are given for the computation of identities (from Formula 1) and roundness measures.

4.4 Computation times and data

The graphics were computed on our personal machines (standard laptops), with simulation times and data presented on Table 3. Details on the implementation (no parallelization) can be found at

https://github.com/huacayacauh/JS-Sandpile/wiki/Roundness.

4.5 Analysis of roundness measures

Well, it appears clearly that the circular shapes observed during the stabilization process $(m + e)^{\circ} = m$ are not asymptotically approaching perfect circles. Indeed, in all experiments conducted on large tilings (Figures 21 and 22), at the beginning of phase 2 the roundness is above the base roundness, whereas the base roundness is an upper bound on the best achievable roundness (see Subsection 4.2).

As the circular shapes shrink, it is normal to see the roundness decrease until the value 0 on configuration m (all plots reach the minimum roundness 0 at stabilization step). On the other hand, it appears that roundness and tiling size are correlated, meaning that as the size of the tiling increases, configurations at the beginning of phase 2 are less round. This is illustrated on Figure 23.

Although they do not tend to perfect circles, we may admit that these shapes are close to be, in regard of tiling sizes (Table 3). Increases of roundness are visible to the naked eye on hexagonal and triangular grids which deviate largely from a perfect circle, but are hardly noticeable without measurements on other tilings. Figure 24 illustrates this with the frontier between outer and inner tiles, on the configuration obtained at the beginning
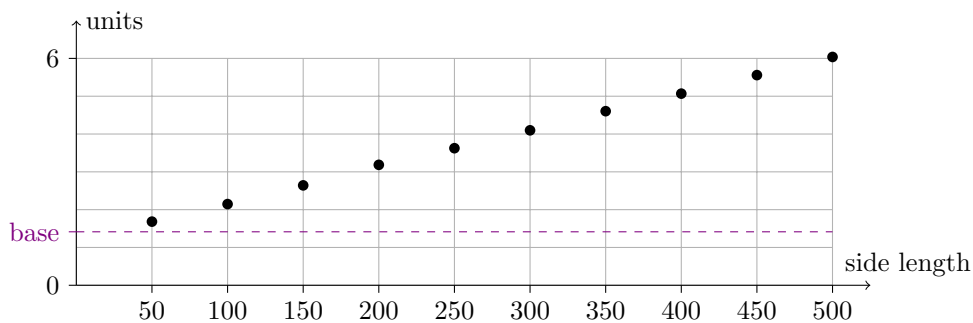
Figure 23: Maximum roundness $\mathbf{r}(c)$ measured during phase 2 of the stabilization process $(m + e)^\circ = m$ on square grids of various side lengths, illustrating the correlation between roundness and size.

of phase 2 during the experiments from Subsection 4.3 (since these configurations are quite large, we picture only the frontier in order to reduce the numerical weight of the present document). If they are not perfect circles, then we may naturally ask: what characterize these frontier shapes for each tiling?

Finally, we see on Figure 24 (first line) that the frontier on grids (respectively square, triangular and hexagonal) reflect the shape on the border of the tilings, somehow "rounded". Indeed, it appears that the number of corners of the grids are equal to the number of parts where the frontier deviates from a circle (the number of times it goes from the inner radius to the outer radius). Theses symmetries are expected, they come from the symmetry of the grids and therefore the symmetries of the dynamics. A natural attempt would be to experiment the roundness of a square grid cropped to a circle, in order to remove the effect of the border's shape. Despite the fact that the difference between the circumscribed and inscribed radius is smaller than the base roundness, this does not lead to significantly smaller roundness measurements (frontiers are not closer to perfect circles) during phase 2 of the stabilization process $(m + e)^\circ = m$, as shown on Figure 25. It feels that the frontier reflects the anisotropy of the square grid itself rather than that of its border's shape.

5 Conclusions and perspectives

The experiments presented in this article are reproducible with *JS-Sandpile* (links in Preamble). The software implements no parallelization mechanism, which would allow to perform larger simulations (*e.g.* using GPU). Nevertheless we believe that this would not lead to qualitatively different observations.

We have presented some identity elements on Penrose tilings, revealing no obvious structure related to these famous aperiodic tilings. Identities are highly sensitive to the shape of the tiling, and it may be the case that other finite croppings of (infinite) Penrose tilings lead to different observations. We tried to build the most "natural" finite Penrose tilings: Suns and Stars obtained by substitution, along with cut and project from a 5-
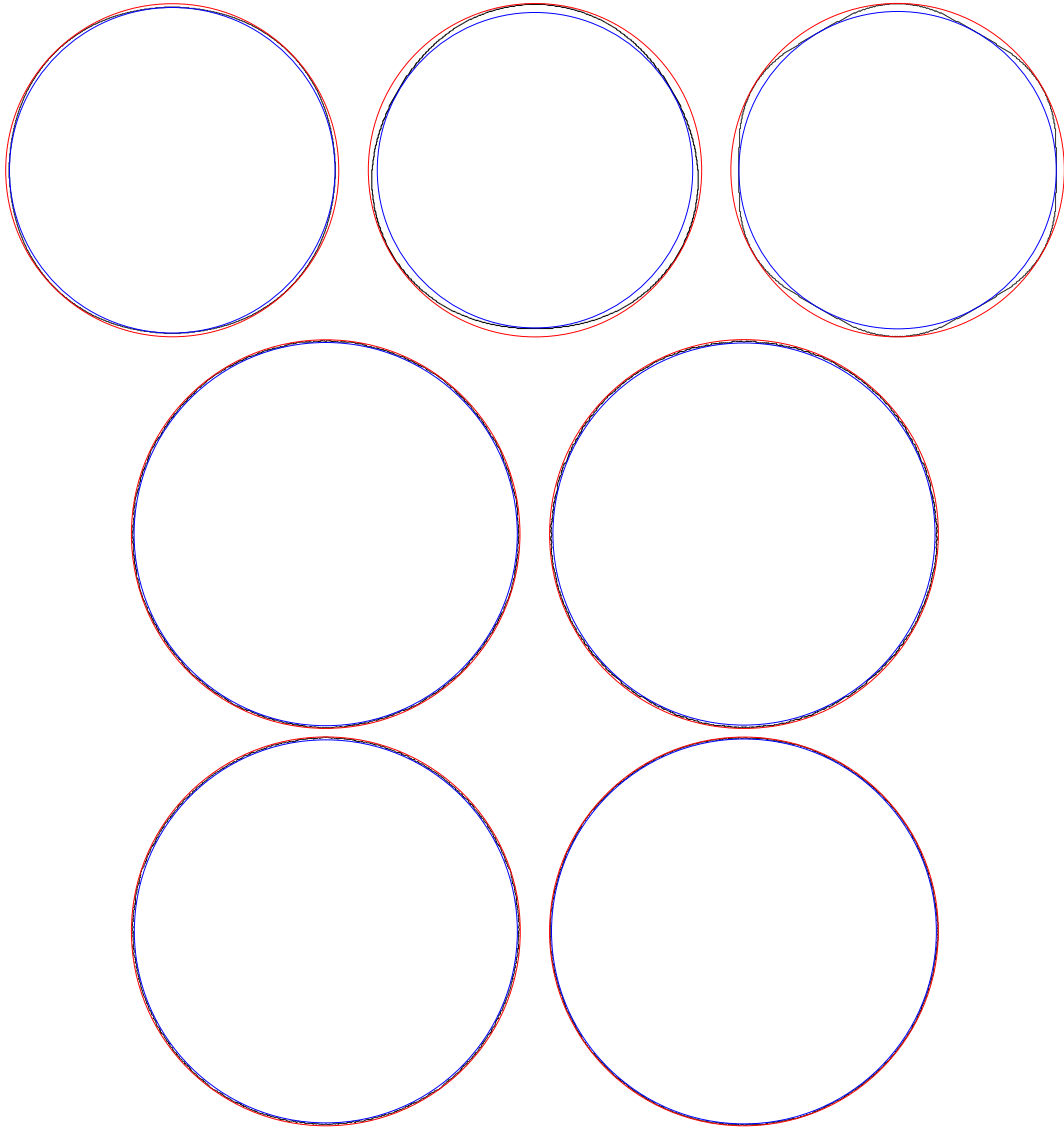
Figure 24: Frontier between inner and outer tiles on the configuration obtained at the beginning of phase 2, as the set of edges shared by one inner tile and one outer tile. Outer radius in blue, inner radius in red. Top: square grid of side length 500 at step 40413 ($\mathtt{r}(c) \approx 5.687$), triangular grid of side length 500 at step 50163 ($\mathtt{r}(c) \approx 7.755$), hexagonal grid of side length 200 at step 13252 ($\mathtt{r}(c) \approx 14.470$). Middle: P2 Sun after 11 iterations of the subsitution at step 42724 ($\mathtt{r}(c) \approx 4.246$), P2 Star after 11 iterations of the subsitution at step 27337 ($\mathtt{r}(c) \approx 4.064$). Bottom: P3 Sun after 10 iterations of the subsitution at step 42067 ($\mathtt{r}(c) \approx 3.220$), P3 Sun cut and project tiling of size 100 at step 39210 ($\mathtt{r}(c) \approx 2.452$).
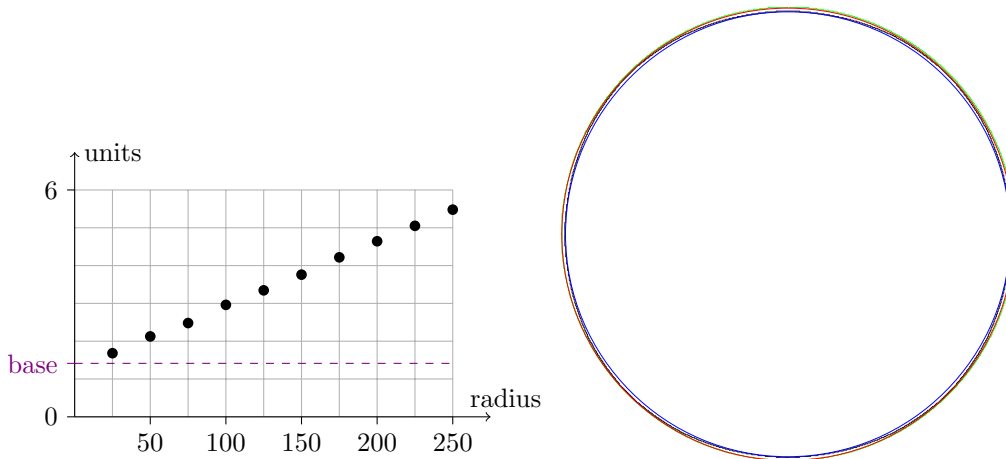
Figure 25: Left: maximum roundness $\mathbf{r}(c)$ measured during phase 2 of the stabilization process $(m + e)^\circ = m$ on square grids cropped to circles of various radii. Right: frontier between inner and outer tiles on the configuration obtained at the beginning of phase 2 (step 32131, $\mathbf{r}(c) \approx 4.073$) on a square grid cropped to a circle of radius 250 (the border of the tiling is pictured in green).

dimensional hypercube.

The apparent isotropy, observed during the stabilization of the maximum stable configuration plus the identity element of the sandpile group, has been measured through the notion of roundness. Experiments revealed that these frontiers are actually not approaching perfect circles on any tiling under consideration. Two further directions may be investigated. First, if these shapes are not perfect circles, then how to characterize them on each tiling (especially on grids)? Second, which tilings would lead to frontiers approaching perfect circles (if any)? The modest attempt to crop a square grid to a circle fails, suggesting that this may not be easy to achieve on tilings which are intrinsically anisotropic at the tile level.

Penrose tilings exhibit frontiers closer to perfect circles, though they also deviate significantly from their best achievable roundness. It is not very surprising to observe on Penrose tilings a behavior similar to regular lattices, as they are quasi-periodic, and in some sense the "most regular" aperiodic tilings. Let us open the large perspective of considering other tilings, for example tilings with higher quasi-periodicity functions (above affine [4, 7, 12][6]), Cayley graphs [53], or hyperbolic planes (*e.g.* with Poincaré disk models).

Finally, could the stabilization process $(m + e)^\circ = m$ shed some light on the enigmatic identity elements on grids? This is really out of reach for our present knowledge, but we hope that the recent progresses of Levine *et al.* [35, 36, 37, 44, 45] are breaking some scientific locks in the domain of sandpiles.

---

[6]The difficulty may be to find constructions from non Wang tiles, because Wang tiles would lead to square grids for the sandpile model to play on (as we remove tile decorations).

Acknowledgments

References

[1] M. Baake, M. Scholottmann, and P. D. Jarvis. Quasiperiodic tilings with tenfold symmetry and equivalence with respect to local derivability. *Journal of Physics A: Mathematical and General*, 24(19):4637–4654, 1991.

[2] P. Bak, C. Tang, and K. Wiesenfeld. Self-organized criticality: An explanation of the $1/f$ noise. *Physical Review Letters*, 59:381–384, 1987.

[3] P. Bak, C. Tang, and K. Wiesenfeld. Self-organized criticality. *Physical Review A*, 38(1):364–374, 1988.

[4] A. Ballier and E. Jeandel. Computing (or not) Quasi-periodicity Functions of Tilings. In *Journées Automates Cellulaires 2010*, pages 54–64, 2010.

[5] R. Berger. The undecidability of the domino problem. *Memoirs of the American Mathematical Society*, 66, 1966.

[6] H. Cairns. Some halting problems for abelian sandpiles are undecidable in dimension three. *SIAM Journal on Discrete Mathematics*, 32(4):2636–2666, 2018.

[7] J. Cervelle and B. Durand. Tilings: recursivity and regularity. *Theoretical Computer Science*, 310(1):469–477, 2004.

[8] N. G. de Bruijn. Algebraic theory of penrose's non-periodic tilings of the plane. ii. *Indagationes Mathematicae*, 84(1):53–66, 1981.

[9] M. Delorme, J. Mazoyer, and L. Tougne. Discrete parabolas and circles on 2D cellular automata. *Theoretical Computer Science*, 218(2):347–417, 1999.

[10] D. Dhar. Self-organized critical state of sandpile automaton models. *Physical Review Letters*, 64:1613–1616, 1990.

[11] D. Dhar, P. Ruelle, S. Sen, and D. N. Verma. Algebraic aspects of abelian sandpile models. *Journal of Physics A*, 28(4):805–831, 1995.

[12] B. Durand. Tilings and quasiperiodicity. *Theoretical Computer Science*, 221(1):61–75, 1999.

[13] J. O. Durand-Lose. Parallel transient time of one-dimensional sand pile. *Theoretical Computer Science*, 205(1-2):183–193, 1998.

[14] V. G. Fast and I. R. Efimov. Stability of vortex rotation in an excitable cellular medium. *Physica D: Nonlinear Phenomena*, 49(1):75–81, 1991.

[15] T. Fernique. *Pavages, Fractions Continues et Géométrie Discrète*. PhD thesis, Université Montpellier II, 2007.

[16] E. Formenti, E. Goles, and B. Martin. Computational complexity of avalanches in the Kadanoff sandpile model. *Fundamenta Informaticae*, 115(1):107–124, 2012.

[17] E. Formenti, B. Masson, and T. Pisokas. Advances in symmetric sandpiles. *Fundamenta Informaticae*, 76(1-2):91–112, 2007.

[18] E. Formenti, K. Perrot, and E. Rémila. Computational complexity of the avalanche problem on one dimensional Kadanoff sandpiles. In *Proceedings of AU-TOMATA'2014*, volume 8996 of *LNCS*, pages 21–30, 2014.

[19] E. Formenti, K. Perrot, and E. Rémila. Computational complexity of the avalanche problem for one dimensional decreasing sandpiles. *Journal of Cellular Automata*, 13:215–228, 2018.

[20] E. Formenti, V. T. Pham, H. D. Phan, and T. H. Tran. Fixed-point forms of the parallel symmetric sandpile model. *Theoretical Computer Science*, 533:1–14, 2014.

[21] Enrico Formenti and Kévin Perrot. How Hard is it to Predict Sandpiles on Lattices? A Survey. *Fondamenta Informaticae*, 171:189–219, 2019.

[22] A. Gajardo and E. Goles. Crossing information in two-dimensional sandpiles. *Theoretical Computer Science*, 369(1-3):463–469, 2006.

[23] E. Goles. Sand pile automata. *Annales de l'institut Henri Poincaré (A) Physique théorique*, 56(1):75–90, 1992.

[24] E. Goles and M. Kiwi. Games on line graphs and sand piles. *Theoretical Computer Science*, 115(2):321–349, 1993.

[25] E. Goles, M. Latapy, C. Magnien, M. Morvan, and H. D. Phan. Sandpile models and lattices: a comprehensive survey. *Theoretical Computer Science*, 322(2):383–407, 2004.

[26] E. Goles, D. Maldonado, P. Montealegre, and N. Ollinger. On the computational complexity of the freezing non-strict majority automata. In *Proceedings of AUTOMATA'2017*, pages 109–119, 2017.

[27] E. Goles and M. Margenstern. Universality of the chip-firing game. *Theoretical Computer Science*, 172(1-2):121–134, 1997.

[28] E. Goles and P. Montealegre. Computational complexity of threshold automata networks under different updating schemes. *Theoretical Computer Science*, 559:3–19, 2014.

[29] E. Goles and P. Montealegre. A fast parallel algorithm for the robust prediction of the two-dimensional strict majority automaton. In *Proceedings of ACRI'2016*, pages 166–175, 2016.

[30] E. Goles, P. Montealegre, K. Perrot, and G. Theyssier. On the complexity of two-dimensional signed majority cellular automata. *Journal of Computer and System Sciences*, 91:1–32, 2017.

[31] E. Goles, P. Montealegre-Barba, and I. Todinca. The complexity of the bootstraping percolation and other problems. *Theoretical Computer Science*, 504:73–82, 2013.

[32] E. Goles, M. Morvan, and H. D. Phan. Sandpiles and order structure of integer partitions. *Discrete Applied Mathematics*, 117(1–3):51–64, 2002.

[33] B. Grünbaum and G. C. Shephard. *Tilings and Patterns*. W. H. Freeman & Co., 1986.

[34] L. P. Kadanoff, S. R. Nagel, L. Wu, and S. Zhou. Scaling and universality in avalanches. *Physical Review A*, 39(12):6524–6537, 1989.

[35] L. Levine, W. Pegden, and C. K. Smart. Apollonian structure in the abelian sandpile. *Geometric and Functional Analysis*, 26:306–336, 2016.

[36] L. Levine, W. Pegden, and C. K. Smart. The apollonian structure of integer superharmonic matrices. *Annals of Mathematics*, 186(1):1–67, 2017.

[37] L. Levine and Y. Peres. Laplacian growth, sandpiles, and scaling limits. *Bulletin of the American Mathematical Society*, 54(3):355–382, 2017.

[38] M. Marek. Grid anisotropy reduction for simulation of growth processes with cellular automaton. *Physica D: Nonlinear Phenomena*, 253:73–84, 2013.

[39] M. Markus and B. Hess. Isotropic cellular automaton for modelling excitable media. *Nature*, 347:56–58, 1990.

[40] P. B. Miltersen. The computational complexity of one-dimensional sandpiles. In *Proceedings of CiE'2005*, pages 342–348, 2005.

[41] C. Moore. Majority-vote cellular automata, Ising dynamics, and P-completeness.

[42] C. Moore and M. Nilsson. The computational complexity of sandpiles. *Journal of Statistical Physics*, 96:205–224, 1999. 10.1023/A:1004524500416.

[43] V.-H. Nguyen and K. Perrot. Any shape can ultimately cross information on two-dimensional abelian sandpile models. In *Proceedings of AUTOMATA'2018*, volume 10875 of *LNCS*, pages 127–142, 2018.

[44] W. Pegden and C. K. Smart. Convergence of the abelian sandpile. *Duke Mathematical Journal*, 162(4):627–642, 03 2013.

[45] W. Pegden and C. K. Smart. Stability of patterns in the abelian sandpile. *Annales Henri Poincaré*, 21:1383–1399, 2020.

[46] R. Penrose. The role of aesthetics in pure and applied mathematical research. *Bulletin of the Institute of Mathematics and Its Applications*, 10(2):266–271, 1974.

[47] R. Penrose. Pentaplexity: A class of non-periodic tilings of the plane. *The Mathematical Intelligencer 2*, pages 32—-37, 1979.

[48] K. Perrot. *Les piles de sable Kadanoff*. PhD thesis, École normale supérieure de Lyon, 2013.

[49] K. Perrot, H. D. Phan, and V. T. Pham. On the set of Fixed Points of the Parallel Symmetric Sand Pile Model. In *Proceedings AUTOMATA'2011*, DMTCS, pages 17–28. Open Publishing Association, 2011.

[50] H. D. Phan. *Structures ordonnées et dynamiques de piles de sable*. PhD thesis, Université Paris 7, 1999.

[51] H. D. Phan. Two sided sand piles model and unimodal sequences. *ITA*, 42(3):631–646, 2008.

[52] R. M. Robinson. Undecidability and nonperiodicity for tilings of the plane. *Inventiones mathematicae*, 12:177–209, 1971.

[53] Zs. Roka. *Automates cellulaires sur graphes de Cayley*. PhD thesis, École Normale Supérieure de Lyon, 1994.

[54] H. E. Schepers and M. Markus. Two types of performance of an isotropic cellular automaton: stationary (Turing) patterns and spiral waves. *Physica A: Statistical Mechanics and its Applications*, 188(1):337–343, 1992.

[55] B. Schönfisch. Anisotropy in cellular automata. *Biosystems*, 41(1):29–41, 1997.

[56] G. Ch. Sirakoulis, I. Karafyllidis, and A. Thanailakis. A cellular automaton for the propagation of circular fronts and its applications. *Engineering Applications of Artificial Intelligence*, 18(6):731–744, 2005.

[57] H. Wang. Proving theorems by pattern recognition — II. *The Bell System Technical Journal*, 40:1–41, 1961.

[58] J. R. Weimar. Cellular automata for reaction-diffusion systems. *Parallel Computing*, 23(11):1699–1715, 1997.

[59] J. R. Weimar, J. J. Tyson, and L. T. Watson. Diffusion and wave propagation in cellular automaton models of excitable media. *Physica D: Nonlinear Phenomena*, 55(3):309–327, 1992.